Micro- and Nanofabrication of Robust Reactive Arrays Based on the Covalent Coupling of Dendrimers to Activated Monolayers

Geerten H. Degenhart, Barbara Dordi, Holger Schönherr,* and G. Julius Vancso*

Materials Science and Technology of Polymers, MESA+ Institute for Nanotechnology and Faculty of Science and Technology, University of Twente, 7500 AE Enschede, The Netherlands

Received February 18, 2004. In Final Form: May 3, 2004

We report on methods to fabricate robust micro- and nanopatterned platforms, comprising high functional group densities and quasi three-dimensional structures, for possible applications in biochip array technologies. For this purpose, amine-terminated poly(amidoamine) (PAMAM) dendrimers were immobilized via amide linkage formation on 11,11′-dithiobis(*N*-hydroxysuccinimidylundecanoate) (NHS-C_{10}) self-assembled monolayers (SAMs) on gold surfaces. The coupling reaction and the resulting assemblies were characterized by grazing incidence reflection Fourier transform infrared spectroscopy, contact angle measurements, X-ray photoelectron spectroscopy (XPS), and atomic force microscopy; the obtained surface coverage values were successfully fitted with a Langmuir isotherm. The fraction of unreacted peripheral primary amine groups of the surface-immobilized PAMAM dendrimers was 28% as determined by XPS analysis of trifluoroacetic anhydride-labeled assemblies. Patterning of the PAMAM dendrimers on NHS-C_{10} SAMs on the micrometer and sub-100-nm scale was achieved by microcontact printing and dip pen nanolithography. The resulting patterns are characterized by their high degree of order and stability of the transferred molecules due to covalent attachment.

Introduction

The analysis of biologically relevant molecules and the corresponding interactions between such molecules have long been recognized as crucial step for a better understanding of, for instance, certain diseases and cell malfunction. Along with gene chip technology,[1−4] significant efforts have been devoted to identifying the function of gene products (proteins) by analyzing the corresponding complementary recognition processes, including protein−protein,[5] protein−DNA,[6] protein−ligand,[7] and protein−RNA interactions.[8] The fabrication of biorelated chips is an area of continuing research activity,[9] and several issues still remain to be addressed in the development of viable chips that possess minimized spot sizes. As a result of limitations of detection, the localized immobilization or functionalization of biomolecules with high densities on solid surfaces is required especially for micrometer- and submicrometer-scale arrays. At the same time, steric hindrance and nonspecific protein binding must be minimized for a sensitive detection of biospecific interactions.

The development of, for example, surface plasmon resonance[10] or electrochemistry-based[11] biosensor and biochip platforms has been intensively pursued to date by employing well-defined composite films, such as alkanethiol-based self-assembled monolayers (SAMs) on gold.[12,13] In these approaches, the ability to introduce versatile chip interfaces and to control immobilization of biomolecules, forming a molecular organized layer, has represented a crucial point. Owing to the interplay of organization on the molecular scale and reactivity in the confinement of organized organic thin films,[14−16] high

* Corresponding authors. E-mail: h.schonherr@utwente.nl (H.S.); g.j.vancso@utwente.nl (G.J.V.). Fax: +31 53 489 3823 (H.S.); +31 53 489 3823 (G.J.V.). Tel.: +31 489 3170 (H.S.); +31 489 2967 (G.J.V.).

(1) Fodor, S. P. A.; Read, J. L.; Pirrung, M. C.; Stryer, L.; Lu, A. T.; Solas, D. *Science* **1991**, *251*, 767−773.

(2) Schena, M.; Shalon, D.; Davis, R. W.; Brown, P. O. *Science* **1995**, *270*, 467−470.

(3) Fodor, S. P. A. *Science* **1997**, *277*, 393−393.

(4) (a) Niemeyer, C. M.; Blohm, D. *Angew. Chem., Int. Ed.* **1999**, *38*, 2865−2869. (b) Perou, C. M.; Sorlle, T.; Elsen, M. B.; van de Rijn, M.; Jeffrey, S. S.; Rees, C. A.; Pollack, J. R.; Ross, D. T.; Johnson, H.; Akslen, L. A.; Fluge, O.; Pergamenschikov, A.; Williams, C.; Zhu, S. X.; Lonning, P. E.; Borresen-Dale, A.-L.; Brown, P. O.; Botstein, D. *Nature* **2000**, *406*, 747−752. (c) Schulze, A.; Downward, J. *Nat. Cell Biol.* **2001**, *3*, E190−E195.

(5) Uetz, P.; Giot, L.; Cagney, G.; Mansfield, T. A.; Judson, R. S.; Knight, J. R.; Lockshon, D.; Narayan, V.; Srinivasan, M.; Pochart, P.; Qureshi-Emili, A.; Li, Y.; Godwin, B.; Conover, D.; Kalbfleisch, T.; Vijayadamodar, G.; Yang, M. J.; Johnston, M.; Fields, S.; Rothberg, J. M. *Nature* **2000**, *403*, 623−627.

(6) Bulyk, M. L.; Gentalen, E.; Lockhart, D. J.; Church, G. M. *Nat. Biotechnol.* **1999**, *17*, 573−577.

(7) (a) MacBeath, G.; Koehler, A. N.; Schreiber, S. L. *J. Am. Chem. Soc.* **1999**, *121*, 7967−7968. (b) Houseman, B. T.; Huh, J. H.; Kron, S. J.; Mrksich, M. *Nat. Biotechnol.* **2002**, *20*, 270−274.

(8) Derrigo, M.; Cestelli, A.; Savettieri, G.; Di Liegro, I. *Int. J. Mol. Med.* **2000**, *5*, 111−123.

(9) (a) MacBeath, G.; Schreiber, S. L. *Science* **2000**, *289*, 1760−1763. (b) Lueking, A.; Horn, M.; Eickhoff, H.; Büssow, K.; Lehrach, H.; Walter, G. *Anal. Biochem.* **1999**, *270*, 103−111. (c) Zhu, H.; Klemic, J. F.; Chang, S.; Bertone, P.; Casamayor, A.; Klemic, K. G.; Smith, D.; Gerstein, M.; Reed, M. A.; Snyder, M. *Nat. Genet.* **2000**, *26*, 283−289.

(10) Knoll, W. *Annu. Rev. Phys. Chem.* **1998**, *49*, 569−638.

(11) (a) Wink, T.; van Zuilen, S. J.; Bult, A.; van Bennekom, W. P. *Analyst* **1997**, *122*, R43−R50. (b) *Biosensor and Chemical Sensor Technology: Process Monitoring and Control*, Rogers, K. R., Mulchandani, A., Zhou, W., Eds.; ACS Symposium Series 613; American Chemical Society: Washington, DC, 1995. (c) Li, J. H.; Yan, J. C.; Deng, Q.; Cheng, G. J.; Dong, S. J. *Electrochim. Acta* **1997**, *42*, 961−967.

(12) (a) Frutos, A. G.; Brockman, J. M.; Corn, R. M. *Langmuir* **2000**, *16*, 2192−2197. (b) Mrksich, M. *Chem. Soc. Rev.* **2000**, *29*, 267−273. (c) Lahiri, J.; Isaacs, L.; Tien, J.; Whitesides, G. M. *Anal. Chem.* **1999**, *71*, 777−790.

(13) Dubois, L. H.; Nuzzo, R. G. *Annu. Rev. Phys. Chem.* **1992**, *43*, 437−463.

(14) Chechik, V.; Crooks, R. M.; Stirling, C. J. M. *Adv. Mater.* **2000**, *12*, 1161−1171.

(15) Dordi, B.; Schönherr, H.; Vancso, G. J. *Langmuir* **2003**, *19*, 5780−5786.

(16) Schönherr, H.; Feng, C. L.; Shovsky, A. *Langmuir* **2003**, *19*, 10843−10851.

10.1021/la049580u CCC: $27.50
Published on Web 06/24/2004

Scheme 1: Schematic Representation of Dendrimer Binding to Activated Ester SAMs[a]

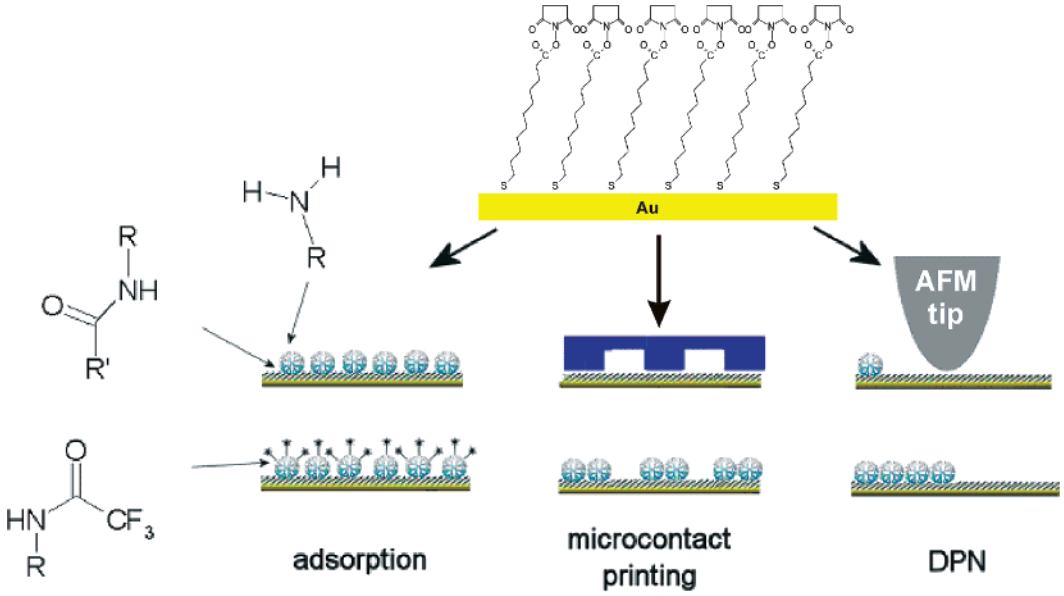

[a] SAMs of NHS-C_{10} were functionalized by covalent coupling of amino terminated dendrimers from solution, by μCP and dip pen nanolithography (DPN), to yield surface-immobilized amide linkages. The number of chemically available primary amino groups was determined by labeling with TFAA in solution.

densities of immobilized biomolecules in their functional form are in certain cases difficult to achieve.[17] To overcome packing constraints and adversely altered reactivity, dendrimers have been recognized as promising elements to fabricate bioreactive organized thin films (vide infra).

Dendrimers belong to a class of monodisperse, synthetic macromolecules with the unusual architecture of a three-dimensional hyperbranched structure[18] and have attracted increasing interest recently, for example, as well-controlled building blocks in bottom-up nanotechnology.[19] Their defined size and structure along with flexible surface functionality makes them promising candidates for numerous applications ranging from chemical sensing to molecular transfer in biological environments.[20] In particular, poly(amidoamine) (PAMAM) starburst dendrimers have shown promising results for the transport of DNA material across cell boundaries.[21]

A number of studies have appeared in the literature describing the immobilization of PAMAM dendrimers onto solid surfaces. These approaches include predominantly multistep wet chemical strategies for immobilization on silica,[22] gold,[23] and mica[24] substrates. The dendrimer layers obtained have several important properties. First, high-generation dendrimers yield quasi three-dimensional surfaces characterized by a higher density of functional groups than found on linear, alkyl-based SAMs.[25] Second, the peripheral functional groups of the dendrimer can be post-functionalized without loss of dendrimers from the surface, which greatly expands their versatility. Third, composite monolayers with properties that are not a simple combination of the individual components can be prepared.

DNA and protein microarray technology require chemically activated surfaces, which allow the highly reproducible and homogeneous coupling of bioorganic compounds.[4] In this context, the versatility of dendrimer-modified silylated glass surfaces has been demonstrated by their employment in the production of both DNA and protein microarrays.[26,27] The dendrimer surfaces obtained by Benters et al., which allow further coupling steps and high stability arising from the covalent attachment to the substrates, will permit the production of dense arrays comprising nucleic acids, proteins, and low-molar-mass compounds.

(17) Spinke, J.; Liley, M.; Schmitt, F. J.; Guder, H. J.; Angermaier, L.; Knoll, W. *J. Chem. Phys.* **1993**, *99*, 7012−7019.
(18) Tomalia, D. A.; Naylor, A. M.; Goddard, W. A., III. *Angew. Chem., Int. Ed. Engl.* **1990**, *29*, 138−141.
(19) (a) Newkome, G. R.; Moorefield, C. N.; Vögtle, F. *Dendritic Molecules: Concepts, Syntheses and Perspectives*; VCH: Weinheim, Germany, 1996. (b) Bosman, A. W.; Janssen, H. M.; Meijer, E. W. *Chem. Rev.* **1999**, *99*, 1665−1688.
(20) (a) Matthews, O. A.; Shipway, A. N.; Stoddart, J. F. *Prog. Polym. Sci.* **1998**, *23*, 1−56. (b) Vögtle, F.; Gestermann, S.; Hesse, R.; Schwierz, H.; Windisch, B. *Prog. Polym. Sci.* **2000**, *25*, 987−1041. (c) Cagin, T.; Wang, G. F.; Martin, R.; Breen, N.; Goddard, W. A. *Nanotechnology* **2000**, *11*, 77−84.
(21) (a) Bielinska, A. U.; Kukowska-Latallo, J. F.; Johnson, J.; Tomalia, D. A.; Baker, J. R., Jr. *Nucleic Acids Res.* **1996**, *24*, 2176−2182. (b) Kukowska-Latallo, J. F.; Bielinska, A. U.; Johnson, J.; Spindler, R.; Tomalia, D. A.; Baker, J. R., Jr. *Proc. Natl. Acad. Sci. U.S.A.* **1996**, *93*, 4897−4899.
(22) (a) Fujiki, K.; Sakamoto, M.; Sato, T.; Tsubokawa, N. *J. Macromol. Sci., Pure Appl. Chem.* **2000**, *37*, 357−377. (b) Baker, L. A.; Zamborini, F. P.; Sun, L.; Crooks, R. M. *Anal. Chem.* **1999**, *71*, 4403−4406. (c) Rubin, S.; Bar, G.; Taylor, T. N.; Cutts, R. W.; Zawodzinski, T. A., Jr. *J. Vac. Sci. Technol., A* **1996**, *14*, 1870−1877. (d) Bar, G.; Rubin, S.; Cutts, R. W.; Taylor, T. N.; Zawodzinski, T. A. *Langmuir* **1996**, *12*, 1172−1179.
(23) (a) Hierlemann, A.; Campbell, J. K.; Baker, L. A.; Crooks, R. M.; Ricco, A. J. *J. Am. Chem. Soc.* **1998**, *120*, 5323−5324. (b) Li, J.; Piehler, L. T.; Qin, D.; Baker, J. R.; Tomalia, D. A.; Meier, D. J. *Langmuir* **2000**, *16*, 5613−5616. (c) Yoon, H. C.; Kim, H. S. *Anal. Chem.* **2000**, *72*, 922−926. (d) Tokuhisa, H.; Zhao, M.; Baker, L. A.; Phan, V. T.; Dermody, D. L.; Garcia, M. E.; Peez, R. F.; Crooks, R. M.; Mayer, T. M. *J. Am. Chem. Soc.* **1998**, *120*, 4492−4501. (e) Hong, M.-Y.; Yoon, H. C.; Kim, H.-S. *Langmuir* **2003**, *19*, 416. (f) Hong, M.-Y.; Lee, D.; Yoon, H. C.; Kim, H.-S. *Bull. Korean Chem. Soc.* **2003**, *24* (8), 1197−1202.
(24) (a) Wells, M.; Crooks, R. M. *J. Am. Chem. Soc.* **1996**, *118*, 3988−3989. (b) Tokuhisa, H.; Crooks, R. M. *Langmuir* **1997**, *13*, 5608−5612.
(25) (a) Ulman, A. *An Introduction to Ultrathin Organic Films*; Academic Press: Boston, 1991. (b) Swalen, J. D.; Allara, D. L.; Andrade, J. D.; Chandross, E. A.; Garoff, S.; Israelachvili, J.; McCarthy, T. J.; Murray, R.; Pease, R. F.; Rabolt, J. F.; Wynne, K. J.; Yu, H. *Langmuir* **1987**, *3*, 932−950.
(26) Benters, R.; Niemeyer, C. M.; Wöhrle, D. *ChemBioChem* **2001**, *2*, 686−694.
(27) Benters, R.; Niemeyer, C. M.; Drutschmann, D.; Blohm, D.; Wöhrle, D. *Nucl. Acid Res.* **2002**, *30* (e10), 1−7.

As we describe in this publication, we developed an alternative methodology to fabricate robust micro- and nanopatterned reactive platforms based on the reaction between amine-terminated PAMAM dendrimers (for structure, see Supporting Information, Scheme S1) and activated SAMs on gold (Scheme 1).

Our approach leads to structurally well-defined assemblies of functionalized and, hence, further reactive dendrimers that are very robust owing to the covalent coupling of the dendrimers to the solid support. High-accuracy monolayer patterns in the micrometer to sub-100-nm range can be fabricated by soft lithography[28] and atomic force microscopy (AFM)-based scanning probe lithography,[29−32] respectively. The large number of chemically accessible functional groups renders this approach an attractive avenue to obtain high areal density (bio)-functionalized arrays.

Experimental Section

Reagents. 11,11′-Dithiobis(*N*-hydroxysuccinimidylundecanoate) (NHS-C_{10}) was synthesized as reported previously.[15] Fourth- and fifth-generation (G_4 and G_5) amine-terminated PAMAM dendrimers were obtained from Aldrich as 10 and 5 wt % methanolic solutions, respectively. Polypropylene imine dendrimers with amine termination [DAB (G_5)], trifluoroacetic acid anhydride (TFAA), and triethylamine (TEA) were purchased from Aldrich. All the organic solvents, except for ethanol (p.a.; Merck), were obtained from Biosolve and used as received.

Monolayer Preparation. All glassware used to prepare monolayers was immersed in piranha solution (solution containing 70% of concentrated sulfuric acid and 30% of hydrogen peroxide) for 15 min, then rinsed with large amounts of high purity water (Millipore Milli-Q water). *Caution: piranha solution should be handled with extreme caution; it has been reported to detonate unexpectedly*. Gold substrates (200-nm gold on 2-nm Ti primer on glass) were purchased from SSENS B.V. (Hengelo, The Netherlands). The substrates were cleaned immediately before use by oxygen plasma (5 min, 30 mA, 60 mTorr; SPI Supplies, Plasma Prep II) and soaked subsequently in ethanol for the same time. The freshly cleaned gold substrates were immersed with minimal delay into 0.1 mM NHS-C_{10} solutions in ethanol. The substrates were removed from solutions after >12 h of assembly time and rinsed extensively with chloroform, ethanol, and water to remove any physisorbed material. Mica substrates were prepared by cleaving the muscovite mica substrates, to produce a clean, smooth surface prior to dip pen nanolithography (DPN) experiments. Silicon substrates were prepared by rinsing Si wafers with ethanol followed by oxygen plasma treatment (5 min, 30 mA, 60 mTorr). The gold substrates used in the microcontact printing (μCP) experiments were obtained from Metallhandel Schröer GmbH (Lienen, Germany). Immediately before use, the substrates were rinsed with Milli-Q water and then flame-annealed in a H_2 flame (purity 6). After the annealing procedure, the substrates were placed in p.a. ethanol for 10 min[33] and then immersed into the NHS-C_{10} solution for the desired time.

Dendrimer Coupling and Kinetics Studies. Dendrimer solutions in methanol were prepared in freshly cleaned glassware with concentrations between 1.0×10^{-3} and 5.0×10^{-10} M. Freshly rinsed SAMs were immersed into the corresponding dendrimer solution, and after a reaction time between 0.5 min to 72 h, they were taken out of solution and thoroughly rinsed with ethanol, water, chloroform, and finally methanol (twice). All experiments were carried out at room temperature, $T = 25 \pm 2$ °C.

Labeling of Dendrimers. A 20-mL solution of 0.1 M TFAA and 0.2 M TEA was prepared in dimethylformamide. The samples were inserted into this solution for 20 min at a temperature of 20 °C. Afterward, the samples were thoroughly rinsed with ethanol, water, chloroform, and finally methanol (twice).

Contact Angle (CA) Measurements. The advancing and receding CAs θ_{adv} and θ_{rec} were measured with Millipore water as a probe liquid by using a CA microscope (Data Physics, OCA 15plus) as reported previously.[15,16]

Polarized Grazing Incidence Reflection Fourier Transform Infrared (GIR−FTIR) Spectroscopy. The FTIR spectroscopy data were collected using a BIO-RAD model FTS575C FTIR spectrometer using a GIR accessory (BIO-RAD) and a liquid nitrogen-cooled cryogenic mercury cadmium telluride detector as reported previously.[15,16] A total of 1024 scans recorded with a resolution of 4 cm^{-1} were ratioed against the previously obtained background spectrum (SAM of d_{33}-hexadecanethiol on gold).

X-ray Photoelectron Spectroscopy (XPS). XPS spectra were recorded on a PHI Quantum 2000 Scanning ESCA microprobe using a monochromated X-ray beam (Al anode). The 100-μm diameter/25-W X-ray beam was scanned over a 1000 μm × 500 μm area at a takeoff angle of 30°. Atomic concentrations were determined by numerical integration of the relative peak areas in the detailed element scans using the following sensitivity factors: C(1s) [0.314], N(1s) [0.499], O(1s) [0.733], and S(2p) [0.717].[34]

AFM. The tapping mode AFM measurements were carried out with a NanoScope III multimode atomic force microscope [Digital Instruments (DI), Santa Barbara, CA] using silicon cantilevers/tips (Nanosensors, Wetzlar, Germany; cantilever resonance frequency $f_0 = 280-320$ kHz). The root-mean-square amplitude of the freely oscillating cantilever was kept constant (1.0 V) for all experiments, and the amplitude damping (setpoint) ratio was adjusted to 0.90. The setup was thermally equilibrated for several hours prior to the measurements to minimize the thermal drift. Contact mode AFM experiments were carried with a NanoScope III multimode atomic force microscope (DI) using V-shaped Si_3N_4 cantilevers (Nanoprobes, DI) with a spring constant of 0.1 N/m. Images were captured in ambient atmosphere (ca. 40−50% relative humidity, 25 °C temperature). To ensure maximum sensitivity for lateral forces in the lateral (friction) force microscopy (LFM) images, the sample was scanned at 90° with respect to the long axis of the cantilever.

μCP. Microcontact-printed substrates were prepared according to literature procedures.[28] Stamps were prepared by casting a 10:1 (v/v) mixture of poly(dimethylsiloxane) and curing agent (Sylgard 184, Dow Corning) against a patterned silicon master. After curing, the stamps were mildly oxidized in an ozone plasma reactor for 30 min and then inked by soaking them in the methanolic adsorbate solution for 5 min. Before printing, the stamps were rinsed with water and blown dry in a stream of N_2. The stamps were applied with a pressure of ∼300 Pa for 60 s on preformed SAMs on gold and then carefully removed. The SAMs were then extensively rinsed with water, ethanol, and methanol.

DPN. To remove surface contaminants, Si_3N_4 tips were immersed in chloroform for 24 h. Cleaned tips were coated with PAMAM dendrimers by soaking them for 1 min in a 0.1 wt % methanolic solution followed by drying. The tip was then scanned twice across a $1 \times 1\ \mu m^2$ area on three different substrates: mica, Si/SiO_2, and NHS-C_{10} SAMs on granular (Piranha-cleaned, but not annealed) gold (scan velocity ∼3 μm/s, $T = 25$ °C, relative humidity 47 ± 3%). To visualize the fabricated pattern in lateral force mode, the scan size was then increased to $5 \times 5\ \mu m^2$, and

(28) (a) Lopez, G. P.; Biebuyck, H. A.; Whitesides, G. M. *Langmuir* **1993**, *9*, 1513−1516. (b) Kumar, A.; Biebuyck, H. A.; Whitesides, G. M. *Langmuir* **1994**, *10*, 1498−1511. (c) Wilbur, J. L.; Kim, E.; Xia, Y.; Whitesides, G. M. *Adv. Mater.* **1995**, *7*, 649−652. (d) Xia, Y.; Whitesides, G. M. *Adv. Mater.* **1995**, *7*, 471−473.

(29) (a) Piner, R. D.; Zhu, J.; Hong, S.; Mirkin, C. A. *Science* **1999**, *283*, 661−663. (b) Ginger, D. S.; Zhang, H.; Mirkin, C. A. *Angew. Chem., Int. Ed.* **2004**, *43*, 30−45.

(30) McKendry, R.; Huck, W. T. S.; Weeks, B.; Fiorini, M.; Abell, C.; Rayment, T. *Nano Lett.* **2002**, *2*, 713−716.

(31) Hyun, J.; Ahn, S. J.; Lee, W. K.; Chilkoti, A.; Zauscher, S. *Nano Lett.* **2002**, *2*, 1203−1207.

(32) Auletta, T.; Dordi, B.; Mulder, A.; Sartori, A.; Onclin, S.; Bruinink, C. M.; Peter, M.; Nijhuis, C. A.; Beijleveld, H.; Schönherr, H.; Vancso, G. J.; Casnati, A.; Ungaro, R.; Ravoo, B. J.; Huskens, J.; Reinhoudt, D. N. *Angew. Chem., Int. Ed.* **2004**, *43*, 369−373.

(33) Ron, H.; Rubinstein, I. *Langmuir* **1994**, *10*, 4566−4573.

(34) The calculated atomic composition is also sensitive to the energy of the primary X-ray beam, variations in the photoionization cross section with chemical structure, the takeoff angle, and the elemental distribution perpendicular to the surface, in addition to the actual composition of the monolayer. Wagner, C. D.; Riggs, W. M.; Davis, L. E.; Moulder, J. F. In *Handbook of X-Ray Photoelectron Spectroscopy*; Muilenberg, G. E., Ed.; Perkin-Elmer Corp.: Eden Prairie, MN, 1979.

Table 1. Advancing and Receding CAs Measured with Water on Different Surfaces

SAM	θ_{adv} [deg]	θ_{rec} [deg]
octadecanethiol	111 ± 3	108 ± 5
11-mercaptoundecanoic acid	<15	<15
NHS-C_{10}	57 ± 3	40 ± 3
NHS-C_{10} + G_4 PAMAM	40 ± 2	<15
NHS-C_{10} + G_5 PAMAM	30 ± 3	<15
NHS-C_{10} + G_5 DAB	44 ± 3	18 ± 3

the scan velocity was set to ~40 μm/s. The 50 ± 20 nm thick lines were produced by scanning each line for a 2-min period (scan velocity of ~4 μm/s, T = 25 °C and relative humidity 39 ± 3%) and the readout was performed increasing the scan size to 4 × 4 μm^2 and the scan velocity to 30 μm/s. The 70 ± 10 nm thick lines were produced by scanning each line for a 2-min period (scan velocity of ~2 μm/s, T = 25 °C and relative humidity 39 ± 3%), and the readout was performed increasing the scan size to 2.5 × 2.5 μm^2 and the scan velocity to 40 μm/s.

Results and Discussion

As we show in the following, amino-group-terminated dendrimers, including G_4 and G_5 PAMAM and G_5 DAB dendrimers, can be immobilized on activated monolayer surfaces in a number of ways. In this study, adsorption from solution phase, μCP, and AFM tip-mediated transfer[29,35] were investigated (Scheme 1). The reaction between *N*-hydroxysuccinimide (NHS) esters in SAMs of NHS-C_{10} with primary amino groups exposed at the periphery of PAMAM and DAB dendrimers was utilized for dendrimer immobilization via covalent (amide) bond formation. Before the fabrication of patterned reactive surfaces is presented, the formation and characterization of neat dendrimer layers by covalent coupling is discussed.

Adsorption of Dendrimers to Activated SAMs. Following the reaction of SAMs of NHS-C_{10} on gold with G_4 PAMAM dendrimers for 24 h in methanol, the dynamic CAs were measured with water as a probe liquid. In Table 1 the CAs are given for a number of NHS SAMs, including neat NHS-C_{10} SAMs reacted with amino-terminated dendrimers, as well as two reference layers. We observe a good correspondence of the methyl-, carboxylic acid-, and NHS-terminated SAMs with values reported in the literature.[15,36] Upon adsorption of G_4 PAMAM on the NHS SAM, a notable decrease in the advancing CA and a very pronounced decrease in the receding CA were observed compared to those of the unreacted NHS SAM. The large hysteresis can be attributed to an increased disorder and mobility present in the organic thin film surface. The data for the G_5 PAMAM and G_5 DAB dendrimers reacted with NHS SAMs are consistent with this interpretation and, thus, indicate that coupling of PAMAM dendrimers to the SAMs occurred.

The second indication for a successful immobilization of G_4 PAMAM on NHS-C_{10} was provided by real-space visualization of the immobilized dendrimers. Using tapping or contact mode AFM, the presence of essentially monodisperse round features was clearly observed for samples after exposure to G_4 PAMAM solutions in methanol. In Figure 1 we compare tapping mode AFM height and phase images of Au(111) covered with NHS-C_{10} after the reaction of G_4 PAMAM. In agreement with previous work on related systems,[37] the individual round features and clusters of features, which are apparent in this Figure, are attributed to individual dendrimers and clusters of dendrimers.

The measured height values of the features attributed to dendrimers of ~2 nm were found in agreement with results reported earlier for PAMAM deposited on mica and gold.[38] The diameter was found to vary between 10 and 15 nm. Considering the theoretical diameter (4.5 nm)[38c] and tip convolution effects, these data are consistent with the interpretation that the features are indeed individual dendrimers.

The coupling of amino-group-terminated dendrimers to NHS ester SAMs was further investigated using GIR-FTIR spectroscopy. There are a number of very characteristic peaks in the IR spectrum of the unreacted SAM, as well as the SAM after reaction with the dendrimers (Figure 2). The peak at 1745 cm^{-1} and a number of peaks in the 1300−1000 cm^{-1} region are characteristic for NHS-C_{10},[15] while two broad amide bands (1665 cm^{-1}) and (1550 cm^{-1}) are present after the reaction with the PAMAM dendrimers. Assuming that the orientation of the corresponding functional groups (dipole transition moments) does not change as a function of the reaction time or surface coverage, the integrated area under the absorption bands can be used to estimate the surface coverage and, hence, the progress of the reaction (vide infra).

The spectra of adsorbed G_4 PAMAM all show strong amide bands and, depending on the reaction time, the disappearance of the succinimide carbonyl band. A large fraction of the amide bands are caused by internal amide bonds of the dendrimers. Owing to the absence of other nucleophiles in the reaction medium, the disappearance of the succinimide carbonyl band suggests the formation of amide linkages between the SAM and the dendrimers.

The bulk IR spectrum of PAMAM (see Supporting Information) represents an isotropic distribution of the dipole transition moments. A comparison of this bulk FTIR and the GIR-FTIR spectra indicates a slight change in the relative integrated absorbances of the peaks assigned to the amide I and II vibrations. In the GIR spectra, the amide I band is lower in integrated absorbance compared to the amide II band. These data are indicative for a slightly preferential in-plane orientation of the C═O bond of the amide groups, which may also be attributed to the formation of covalent bonds with the reactive SAM.

However, G_4 PAMAM dendrimers contain many internal amide bonds (124 bonds vs 64 peripheral primary amino groups); thus, it is difficult to estimate how far the dendrimer is covalently bonded to the SAM. To circumvent this problem, we investigated the reaction with DAB dendrimers. Unlike PAMAM, DAB dendrimers do not contain any amide bonds.

In Figure 3, the GIR-FTIR spectrum of surface-immobilized DAB dendrimers is shown. The amide I and amide II bands at 1665 and 1550 cm^{-1}, respectively, are clearly present. These amide bands are attributed to the covalent bond formation between amine and NHS ester groups because there are no amide bonds present in the

(35) Jaschke, M.; Butt, H.-J. *Langmuir* **1995**, *11*, 1061−1064.
(36) Bain, C. D.; Troughton, E. B.; Tao, Y.-T.; Evall, J.; Whitesides, G. M.; Nuzzo, R. G. *J. Am. Chem. Soc.* **1989**, *111*, 321−335.
(37) (a) Huisman, B.-H.; Schönherr, H.; Huck, W. T. S.; Friggeri, A.; van Manen, H.-J.; Menozzi, E.; Vancso, G. J.; van Veggel, F. C. J. M.; Reinhoudt, D. N. *Angew. Chem., Int. Ed.* **1999**, *38*, 2248−2251. (b) Friggeri, A.; van Manen, H.-J.; Auletta, T.; Li, X.-M.; Zapotoczny, S.; Schönherr, H.; Vancso, G. J.; Huskens, J.; van Veggel, F. C. J. M.; Reinhoudt, D. N. *J. Am. Chem. Soc.* **2001**, *123*, 6388−6395. (c) van Manen, H.-J.; Auletta, T.; Dordi, B.; Schönherr, H.; Vancso, G. J.; van Veggel, F. C. J. M.; Reinhoudt, D. N. *Adv. Funct. Mater.* **2002**, *12*, 811−818.
(38) (a) Müller, T.; Yablon, D. G.; Karchner, R.; Knapp, D.; Kleinman, M. H.; Fang, H.; Durning, C. J.; Tomalia, D. A.; Turro, N. J.; Flynn, G. W. *Langmuir* **2002**, *18*, 7452−7455. (b) Betley, T. A.; Banaszak Holl, M. M.; Orr, B. G.; Swanson, D. R.; Tomalia, D. A.; Baker, J. R., Jr. *Langmuir* **2001**, *17*, 2768−2773. (c) Lackowski, W. M.; Campbell, J. K.; Edwards, G.; Chechik, V.; Crooks, R. M. *Langmuir* **1999**, *15*, 7632−7638.

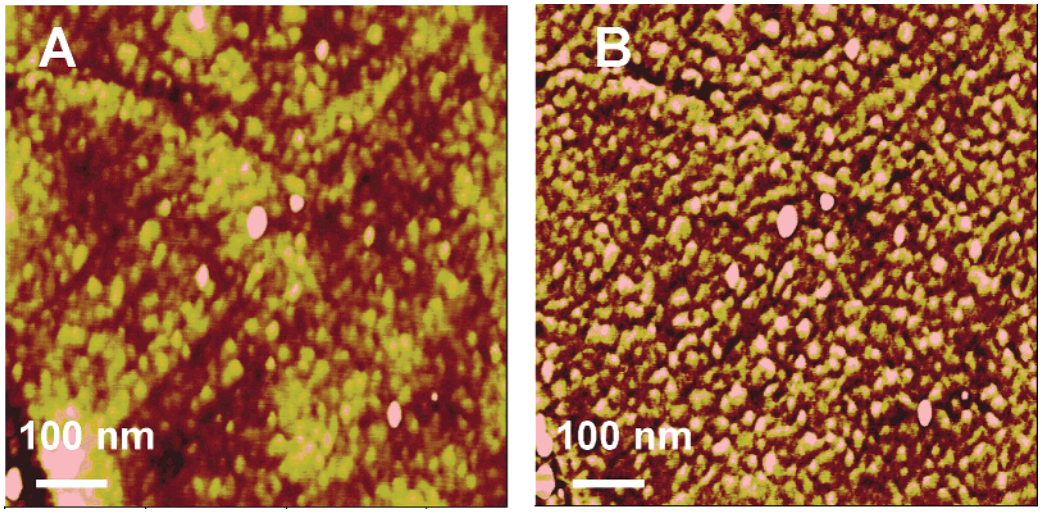

Figure 1. Tapping mode AFM height image (A, acquired in air, z scale = 5.0 nm) and phase image (B) of the NHS-C_{10} SAM fully covered with G_4 PAMAM. The triangular terraces of Au(111) are clearly recognized in the height image (left), indicating that a layer of homogeneous thickness has been deposited.

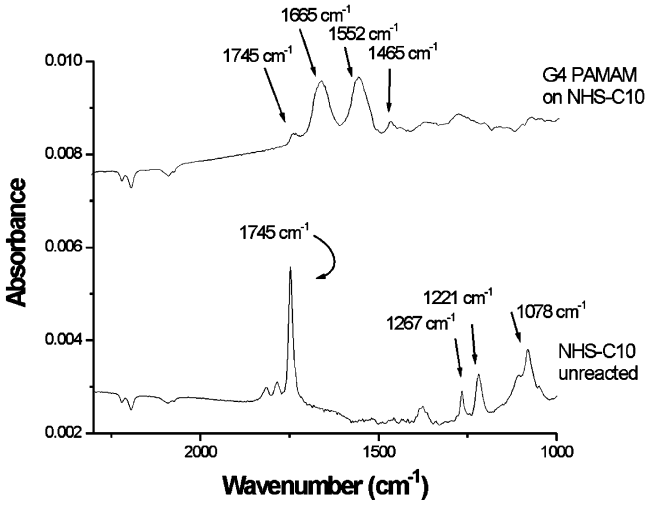

Figure 2. GIR-FTIR spectrum of G_4 PAMAM reacted with the SAM of NHS-C_{10} (top) and neat SAM of NHS-C_{10} (bottom). The characteristic peaks observed for G_4 PAMAM reacted with the SAM of NHS-C_{10} at 1665 and 1550 cm^{-1} are attributed to the amide I and amide II vibrations, respectively. The unreacted SAM shows a number of characteristic bands, most prominently the narrow succinimide carbonyl band at 1745 cm^{-1}.

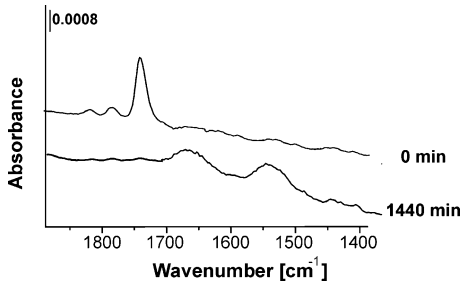

Figure 3. GIR-FTIR spectra of the NHS-C_{10} SAM before and after reaction with DAB-G_5, in 1.0×10^{-5} M methanolic solution of DAB-G_5. The amide I (1665 cm^{-1}) and II (1550 cm^{-1}) bands are clearly visible beside the NHS carbonyl vibration (1745 cm^{-1}).

DAB dendrimers. On the basis of the observation that DAB dendrimers are bound covalently, we assume that PAMAM dendrimers do so as well.

Next, the kinetics of the PAMAM coupling reaction was analyzed in detail. The progression of the coupling reaction

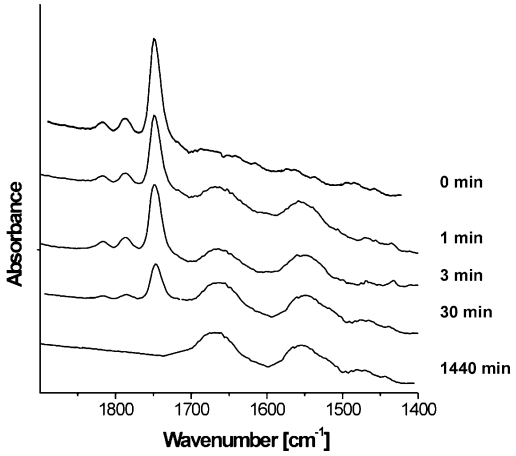

Figure 4. GIR-FTIR spectra of the NHS-C_{10} SAM after reaction with G_4 PAMAM dendrimers for various times (4.5×10^{-6} M methanolic solution of G_4 PAMAM).

was followed by GIR-FTIR spectroscopy. These measurements were performed in an ex situ mode for samples immersed in the appropriate methanolic solutions for variable periods of time followed by extensive rinsing. Figure 4 shows the carbonyl region of the spectra at different stages of the reaction. The strong band at 1745 cm^{-1}, assigned to succinimidyl carbonyl, ν(C═O), decreases in absorbance with the progress of the reaction, while the amide I and amide II bands at about 1665 and about 1555 cm^{-1} increase in absorbance.

On the basis of the FTIR data (Figure 4), the coverage θ can be expressed as a function of the reaction time. The surface coverage θ can be obtained as

$$\theta = A_t/A_\infty \qquad (1)$$

where A_t is the sum of integrated absorbance of the amide I and amide II bands at time t and A_∞ is at infinite time, respectively.

In Figure 5, results obtained for three different concentrations of dendrimers are shown. The surface coverage of dendrimers increases rapidly in the early stages of adsorption and then slows before going to completion.

A well-known model to describe adsorption, for instance, of dendrimers to solid substrates, is the Langmuir

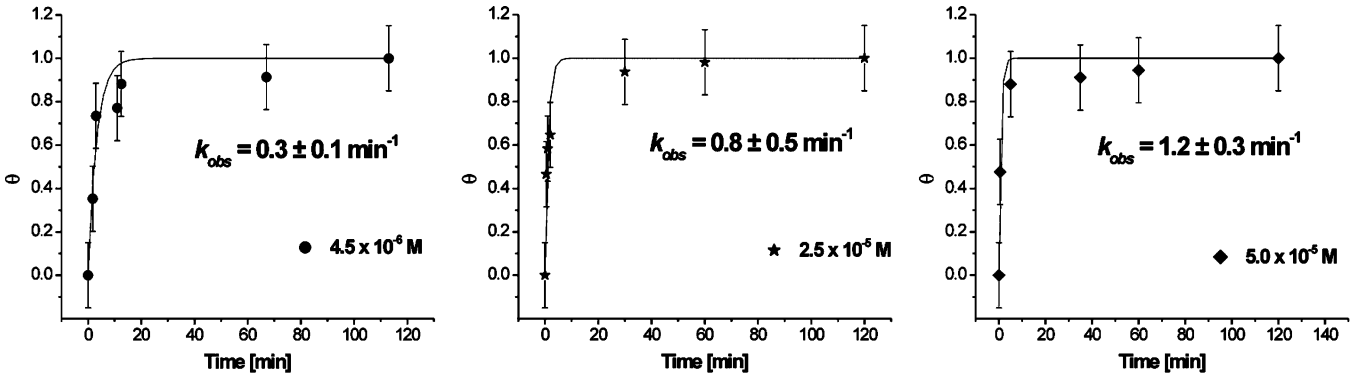

Figure 5. Plot of normalized surface coverage θ as function of reaction time t for the coupling of G_4 PAMAM with NHS-C_{10}, as determined by GIR-FTIR spectroscopy. The solid line corresponds to the fit of the Langmuir model according to eq 4.

monolayer adsorption model.[39] The Langmuir model is based on the assumptions that adsorption is limited to one monolayer, all surface sites are equivalent, and adsorption to one site is independent of the occupancy condition of the adjacent sites. Assuming that we rapidly establish thermodynamic equilibrium (physisorption) before the assembly is covalently bound to the activated SAM, the kinetic constants were determined from our data using the Langmuir model (vide infra).[40]

The surface coverage θ can be expressed as[39]

$$\theta = \frac{k_a C}{k_a C + k_d}\{1 - \exp(-k_{obs} t)\} \qquad (2)$$

where k_a and k_d are the intrinsic rate constants of adsorption and desorption, respectively, and C is the concentration of adsorbate, with

$$k_{obs} = k_a C + k_d \qquad (3)$$

If the desorption process in negligible, that is, $k_d \ll k_a$, eq 2 can be written as

$$\theta = 1 - \exp(-k_{obs} t) \qquad (4)$$

The raw data were fitted to eq 4**,** and the agreement between the fit and the data is shown in Figure 5. From the concentration dependence of k_{obs}, the value of k_a was determined by linear regression analysis to be $(2.0 \pm 0.7) \times 10^4$ min^{-1} M^{-1} (see Figure S3, Supporting Information).

In a separate set of similar experiments, the adsorption of the G_4 PAMAM dendrimers was investigated at a fixed time and varying concentration. It was found that very low concentrations still produce fully covered layers. The steady-state fractional coverage of the surface is given by the Langmuir isotherm:[39]

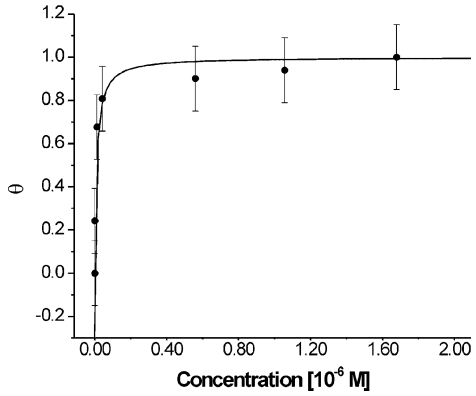

Figure 6. Adsorption isotherm of G_4 PAMAM on NHS-C_{10}. The solid line corresponds to the fit of the Langmuir isotherm according to eq 5.

$$\theta = \frac{K_{eq} C}{1 + K_{eq} C} \qquad (5)$$

Figure 6 shows the adsorption isotherm of G_4 PAMAM dendrimers on NHS-C_{10}. The data could be fitted with eq 5 and gave an equilibrium complexation constant ($K_{eq} = k_a/k_d$) of $(8.7 \pm 2.6) \times 10^7$ M^{-1}.

From a comparison of the equilibrium constant K_{eq} and the adsorption constant k_a, the value for k_d is found as $(2.3 \pm 1.5) \times 10^{-4}$ min^{-1}. This value, as well as the values for k_d and K_{eq}, are constants determined on the basis of the Langmuir model. Although these constants provide a good indication of the adsorption process (most importantly in the early phases of adsorption), the Langmuir model may not correctly describe the entire process. Notwithstanding this, our results allow one, in principle, to predict/control the coverage of G_4 PAMAM on the NHS-C_{10} SAM by variations of concentration or adsorption time.

To quantify the number of covalent bonds formed between each dendrimer and the activated SAM, as well as to estimate the number of surface-exposed chemically accessible primary amino groups per dendrimer, we investigated TFAA-labeled specimens by XPS (Scheme 1).

For this purpose, NHS-C_{10} SAMs were reacted with G_4 and G_5 PAMAM. The conditions used for dendrimer adsorption led to an equilibrium state with a maximum attainable surface occupation of dendrimers. Subse-

(39) (a) Karpovich, D. S.; Blanchard, G. J. *Langmuir* **1994**, *10*, 3315−3322. (b) Hu, K.; Bard, A. J. *Langmuir* **1998**, *14*, 4790−4794. (c) Lahiri, J.; Isaacs, L.; Grzybowski, B.; Carbeck, J. D.; Whitesides, G. M. *Langmuir* **1999**, *15*, 7186−7198. (d) Schouten, S.; Stroeve, P.; Longo, M. L. *Langmuir* **1999**, *15*, 8133−8139.

(40) The support for the notion that the covalent attachment may not occur instantaneously is twofold. First, we have observed a very much hindered reaction of *n*-butylamine with NHS-C_{10}. In particular, the presence of an induction period detected by contact angles, FTIR, and inverted chemical force microscopy indicates that the rate of the reaction increases after ~10 min under the conditions employed. Dordi, B.; Pickering, J. P.; Schönherr, H.; Vancso, G. J. *Eur. Polym. J.* **2004**, *40*, 939−947. Second, the absorbance of the succinimide ester band in a SAM of NHS-C_{10} covered with a multilayer of G_4 PAMAM was pronounced after preparation and vanished completely after storage of the sample overnight (see Figure S2, Supporting Information). Hence, we concluded that a post-assembly completion of the covalent attachment reaction may occur.

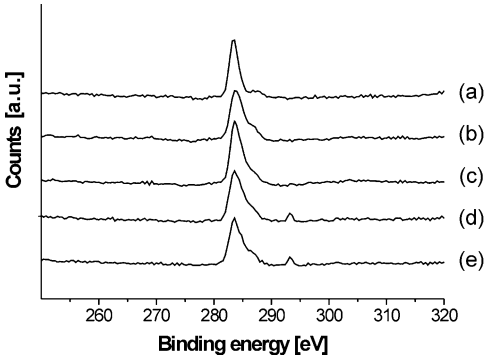

Figure 7. C(1s) XPS spectra of (a) NHS-C_{10} SAM; (b) NHS-C_{10} SAM functionalized with a 5.5×10^{-5} M solution of G_4 PAMAM; (c) NHS-C_{10} SAM functionalized with a 2.7×10^{-5} M solution of G_5 PAMAM; (d) following reaction of specturm b with TFAA; (e) following reaction of spectrum c with TFAA.

Table 2. Atomic Composition (with Standard Deviation σ) of Various Unlabeled and Trifluoro-Labeled SAMs As Determined by XPS

	C	N	O	F	S
NHS-C_{10}	78.1	4.1	14.2		3.6
σ	3.7	2.0	1.8		0.1
NHS-C_{10} + G_4	66.8	13.7	17.5		2.0
σ	4.0	3.0	2.0		0.5
NHS-C_{10} + G_5	71.5	11.6	14.8		2.1
σ	1.9	2.6	0.8		0.2
NHS-C_{10} + G_4 + F	71.4	11.0	13.1	2.4	2.0
σ	0.1	0.2	0.1	0.2	0.2
NHS-C_{10} +G_5 + F	70.8	11.0	13.6	2.4	2.2
σ	0.3	0.2	0.3	0.1	0.1

quently, both dendrimer-functionalized SAMs were immersed in a 0.1 M solution of TFAA for 20 min.[41]

The XPS results confirmed the presence of the expected elements in the monolayers. In particular, the CF_3 functionality in the C1(s) XPS spectra (Figure 7) at 293 eV and the F(1s) signal at 687 eV (see Supporting Information) confirmed the presence of fluorine in the labeled specimens.

The dendrimer species contribute three types of carbon functionality to the C(1s) spectra:[42] carbon singly bonded to an amide carbon/amine nitrogen (C—C—NHR(=O)/C—N ~ 285.7 eV), carbon singly bonded to an amide nitrogen ($-CH_2-NH-C=O$ ~ 286.0 eV), and an amide group (RHN—C=O ~ 287.9 eV). These gave rise to a change of the amide group C(1s) signal (RHN—C=O ~ 287.9 eV) in the NHS-C_{10} SAM. Table 2 presents the results obtained by XPS measurements.

The nitrogen-to-sulfur ratio varied from 1.13 in the case of pure NHS-C_{10} to 5.1 and 5.5 in the case of G_4- and G_5-modified NHS-C_{10}, respectively. After reaction with TFAA, the value was found to be 5.5 for both dendrimers. This ratio did not change significantly because there is no change in the number of nitrogens present on the layer after reaction with TFAA.

As mentioned, the presence of fluorine on the layer after the labeling reaction indicated that the dendrimers had reacted with TFAA, according to Scheme 1. By considering the stoichiometry of the reaction between the free amino groups and TFAA (three fluorine atoms per reacted primary amino group) and by assuming that the TFAA labeling proceeds quantitatively, it is thus possible to estimate the percentage of amino groups available for further functionalization N_x. One-third of the atom percent observed for fluorine provides the atom percent of addressable primary amino groups N_F, while the atom percent of nitrogen represents the content of all amino groups N_N.

The total number of nitrogen atoms in the G_4 (G_5) PAMAM dendrimers includes both nitrogen atoms present in the N_p free peripheral primary amino groups, that is, 64 (128), and the nitrogen atoms present inside the dendrimers. In total, the dendrimers contain N_{tot}, that is, 250 and 506, respectively, nitrogen atoms.

Thus, the percentage of amino groups available for further functionalization N_x can be expressed as

$$N_x = (N_{tot} N_F / N_N)/N_p \qquad (6)$$

In both cases (G_4, G_5), the corresponding percentage of free accessible amino groups N_x was found to be ~28% of the total peripheral primary amino groups of the dendrimers.

The area that one amino group would occupy in a closely packed amino-terminated alkanethiol SAM corresponds to $\sim 2.5 \times 10^{-19}$ m^2/molecule.[43] Considering a G_4 PAMAM dendrimer as an idealized sphere, the area requirement for each chemically accessible amino group is $\sim 8.9 \times 10^{-19}$ m^2. For a G_5 dendrimer layer, the area requirement per free amino group would become $\sim 6.4 \times 10^{-19}$ m^2, which indicates already an increase of density of reactive groups compared to G_4 of ~40%.[44] Interestingly, the area per peripheral amino group that *cannot* be labeled by TFAA for the G_5 dendrimers corresponds roughly to the area requirement per thiol molecule in a functionalized SAM.[43] This result is consistent with a high degree of covalent attachment to the underlying SAM.

The area per active peripheral amino group for G_5 is still larger compared to a tightly packed amino-terminated SAM. However, in contrast to a dendrimer layer,[26] such a tightly packed SAM can be expected to show significantly hindered reactivity in surface coupling reactions and, thus, incomplete conversion, judging from simple model reactions on related SAMs[15,16,45] and optimized surface coverages for the biofunctionalization in mixed monolayers on Au.[17] Further, if one considers higher-generation dendrimers, that is, G_6—G_{10}, the area per reactive amino group decreases progressively as a result of the over-proportional increase in the number of amino groups compared to the increase in the diameter of the dendrimers. This indicates that it is possible to achieve a further increase in the number of reactive groups, that is, a much higher density of reactive groups.

Patterning of SAMs. In addition to a characterization of the coupling process of dendrimers to NHS-terminated SAMs, a second important main aim of this study was to explore possibilities to fabricate well-defined, micro- and submicrometer reactive patterns of the dendrimers. In this process, we intend to take advantage of the robustness of the assemblies given by the covalent attachment of the dendrimers to the NHS-C_{10} SAMs.

(41) Yan, L.; Marzolin, C.; Terfort, A.; Whitesides, G. M. *Langmuir* **1997**, *13*, 6704—6712.

(42) Beamson, G.; Briggs, D. *High-Resolution XPS of Organic Polymers*; Wiley: Chichester, 1992.

(43) Nelles, G.; Schönherr, H.; Jaschke, M.; Wolf, H.; Schaub, M.; Küther, J.; Tremel, W.; Bamberg, E.; Ringsdorf, H.; Butt, H.-J. *Langmuir* **1998**, *14*, 808—815.

(44) The area occupied by a NH_2 group in an amine-terminated SAM is ~25 Å^2; the nominal diameters of G_4 and G_5 are 4.5 and 5.4 nm, respectively. By assuming a spherical shape for the dendrimers, it is possible to calculate the cross section of each generation. By then dividing by the number of chemically addressable amino groups determined by XPS, the area occupied by each amino group is obtained.

(45) (a) Dordi, B. Ph.D. Thesis, University of Twente, Enschede, The Netherlands, 2003. (b) Dordi, B.; Pickering, J. P.; Schönherr, H.; Vancso, G. J. *Surf. Sci.* **2004**, in press.

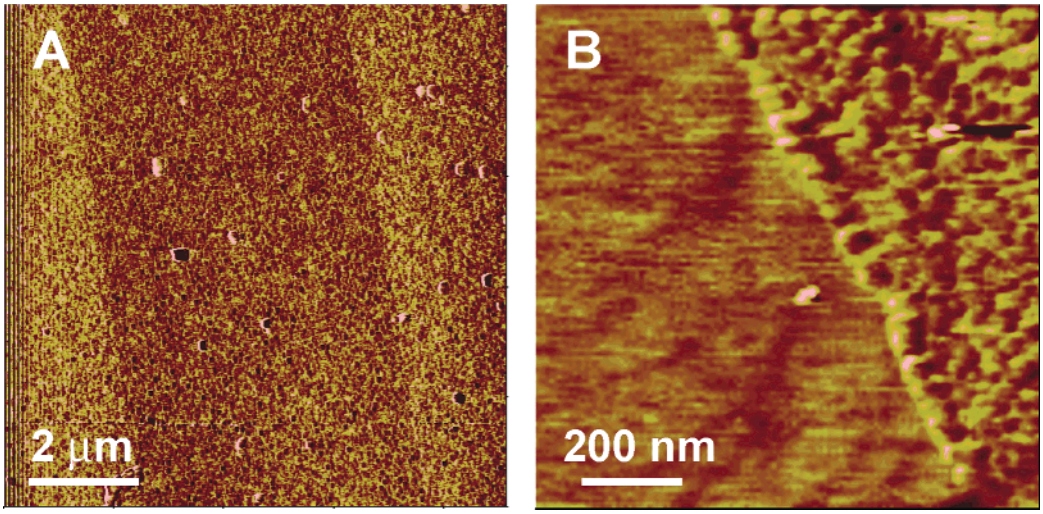

Figure 8. LFM images of the NHS-C_{10} SAM patterned with G_4 PAMAM by μCP (acquired in air; friction forces [a.u.] increase from dark to bright contrast). In the lower resolution image obtained on granular gold (left), the low-friction areas correspond to the bare NHS-C_{10} SAM and the high-friction areas correspond to the immobilized dendrimers. The image shown on the right-hand side was obtained on a pattern fabricated on an atomically flat Au(111) sample.

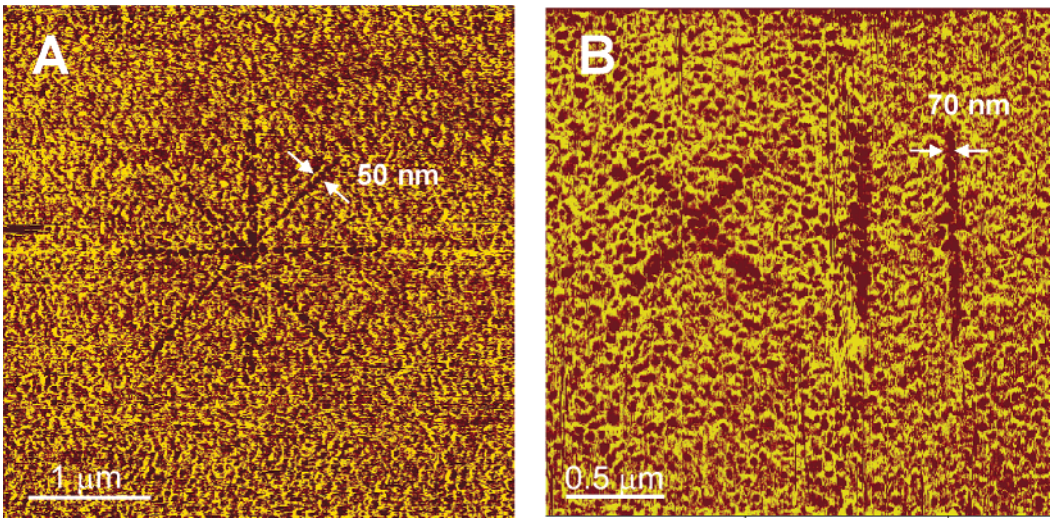

Figure 9. Sequence of LFM force images (acquired in air; friction forces [a.u.] increase from dark to bright contrast) of arrays of lines with mean widths (±standard deviation) of 50 ± 20 nm and 70 ± 10 nm produced by DPN of G_4 PAMAM dendrimers on NHS-C_{10} SAMs on granular gold. The contrast in the LFM scans is reversed compared to the microcontact-printed patterns, which were scanned with a clean Si_3N_4 tip. As also observed in an independent study,[32] the remaining "ink" on the AFM tip used for DPN alters the relative magnitude of the friction forces in this situation.

To microfabricate dendrimer patterns by direct transfer of dendrimers to the activated SAM, we employed soft lithography, in particular μCP,[28] and AFM tip-mediated transfer (DPN) with G_4 PAMAM as the ink and a SAM of NHS-C_{10} as the substrate. In Figure 8, we show AFM images of a microcontact-printed pattern of G_4 PAMAM dendrimers printed onto a NHS-C_{10} SAM, as well as a high magnification of the border between deposited dendrimers and bare SAM.

The LFM image (Figure 8A) shows a line of 5 μm, which appears darker (lower friction forces) than the surrounding areas. The stamp used had lines with widths of 10 μm and interline widths of 5 μm; therefore, the darker area corresponds to the NHS-C_{10} layer that was not in contact with the stamp. The brighter (high friction) areas correspond to the transferred dendrimers. In high-magnification images (Figure 8B) obtained on flat Au(111), it was possible to observe that the amine-terminated dendrimers formed a very uniform layer on the surface of the NHS-C_{10} SAM. We observed many densely packed globular particles and only few irregular clusters. Each of the bright spots may represent a single dendrimer molecule. The edge of the stamped area is very sharp (edge roughness < apparent width of a single dendrimer), which indicates that little molecular surface diffusion occurred during or after printing. This image was captured more than 24 h after printing. Thus, the deposited dendrimers did not diffuse more than a few nanometers from this line. Apparently there are no loosely bound dendrimers, for example, in the form of multilayers present, which are free to diffuse over the surface and bind covalently later.

The ease of printing with dendrimers and the high level of definition of the transferred pattern indicates that μCP with this high-molecular weight "ink" provides an interesting route to patterning with possibly submicrometer features. The diffusion of the "ink" is strongly minimized compared to low-molar-mass inks and, in principle, a higher resolution can be achieved. Our data agree with results reported by the group of Reinhoudt, who used

"heavyweight" molecules,[46] and by Huck and co-workers, who studied μCP with dendrimers on silicon substrates.[47] Hence, the simple and cost-effective fabrication of functionalized high-definition arrays appears to be possible using μCP.

Using the DPN technique,[29] this patterning can be extended to sub-100-nm-sized patterns. Patterns deposited onto silicon or mica showed only limited stability and degree of definition (see Supporting Information, Figure S5). In the case of mica and Si/SiO_2, the originally drawn square was detectable; however, the images showed that dendrimer molecules have likely diffused on the substrates. This could be caused by the shear force exerted by the AFM tip during the scanning or by the fact that the dendrimers were simply physisorbed and could freely diffuse on the surface.

When a NHS-C_{10} SAM on (granular) gold was used as a substrate in a DPN experiment, results were found to be markedly different (see also Figure S5, Supporting Information). Stable patterns were observed in LFM scans. The formation of pattern sizes in the sub-100-nm range was achieved by scanning an AFM tip inked with G_4 PAMAM dendrimers (5.6×10^{-5} M methanolic solution) over a NHS-C_{10} SAM by means of DPN. In Figure 9A, a LFM image of lines 2-μm long and 50 ± 20 nm wide is reported; in Figure 9B, the lines are 1-μm long and 70 ± 10 nm wide.

The pattern deposited by DPN was clearly retained, even after repetitive scans by AFM. Hence, the patterns were proven to be stable, and, hence, we concluded that unlike for silicon and mica the dendrimer molecules were firmly attached to the underlying SAM. This observation supports our strategy that the covalent attachment of the dendrimers via amide bond formation is beneficial to obtain very *robust* assemblies, which is required in potential applications to be compatible with harsher washing steps. Because the dendrimers provide a more open structure and a more solvated environment, we expect that their reactivity is not adversely affected to the same degree as found for tightly packed monolayer architectures.[14−17] Hence, the number of fully reactive functional groups per unit area is likely improved as well.

(46) Liebau, M.; Huskens, J.; Reinhoudt, D. N. *Adv. Funct. Mater.* **2001**, *11*, 147−149.

(47) Li, H.; Kang, D.-J.; Blamire, M. G.; Huck, W. T. S. *Nano Lett.* **2002**, *2*, 347−349.

Conclusions

We have shown that NHS-C_{10} SAMs can be easily and rapidly functionalized with PAMAM dendrimers via amide linkage formation. Compared to previously reported results,[4,27] our alternative approach avoids several time-consuming modification steps and offers a reproducible and quantifiable coupling procedure on gold surfaces. Furthermore, we have proven that the modified surfaces obtained are robust and homogeneously chemically activated (28% of the primary amino groups can be derivatized by TFAA labeling in solution), which is a crucial point in applications, such as DNA or protein microarrays. By means of soft lithographic techniques, such as μCP and DPN, we have highlighted that it is possible to create patterns with (sub-)micrometer resolution and to simultaneously design and control the chemical functionality of the deposited area. The resolution obtained in our work is probably limited only by the size of the stamp and by the scanned area in DPN.

Acknowledgment. The authors thank Alexander Shovsky for his contribution of additional CA measurements and fruitful discussions. This work has been financially supported by the MESA$^+$ Institute for Nanotechnology of the University of Twente and the Council for Chemical Sciences of The Netherlands Organization for Scientific Research (CW-NWO; B.D.) and also in the framework of a vernieuwingsimpuls project (H.S.).

Supporting Information Available: Structures of adsorbate (NHS-C_{10}) and G_4 PAMAM dendrimer, transmission FTIR spectrum of G_4 PAMAM, FTIR spectra of a dendrimer multilayer, concentration dependence of k_{obs} for G_4 PAMAM, XPS survey scans, and LFM images. This material is available free of charge via the Internet at http://pubs.acs.org.

LA049580U